Materials Today Communications 42 (2025) 111418

Contents lists available at ScienceDirect

Materials Today Communications

journal homepage: www.elsevier.com/locate/mtcomm

Biobased composite fibrous membrane using PLA and lignin carbon dots fabricated via solution blow spinning for wound dressing application

Patrícia F. Rossi [a,b], Danilo M. dos Santos [b], Crisiane A. Marangon [b], Kelcilene B.R. Teodoro [b], Camila S. Costa [c], Natália M. Inada [c], Daniel S. Correa [b,*], Rodrigo L. Oréfice [a,*]

[a] Federal University of Minas Gerais (UFMG), Department of Metallurgical and Materials Engineering, Av. Antônio Carlos, 6627, Pampulha, Belo Horizonte, MG 31270-901, Brazil
[b] Nanotechnology National Laboratory for Agriculture (LNNA), Embrapa Instrumentation, Rua XV de Novembro, 1452, São Carlos, SP 13560-979, Brazil
[c] University of São Paulo (USP), São Carlos Institute of Physics (IFSC), Av. Trabalhador São Carlense, 400, Parque Arnold Schimidt, São Carlos, SP 13566-590, Brazil

ARTICLE INFO

Keywords:
Solution blow spinning
Curcumin
Lignin carbon dots
Antibacterial activity
wound dressings
biomaterial
electrical impedance

ABSTRACT

Traditional wound dressings have limitations in terms of their antibacterial and anti-inflammatory properties, as well as their ability to maintain a moist wound environment. Addressing these shortcomings in conventional medical materials is essential for advancing wound healing in clinical applications. Additionally, biodegradable polymeric wound dressings have gained significant attention as a promising solution to reduce the environmental impact associated with the disposal of wound dressings. In this study, we developed a nanoengineered wound dressing fabricated by solution blow spinning technique by using poly(lactic acid) (PLA) fibrous mats that integrate lignin-derived carbon dots (LCDots), further enhanced with curcumin. This unique combination leverages the antimicrobial and antioxidant properties of curcumin alongside the electrical and photoluminescent features of LCDots, creating a multifunctional dressing with enhanced wound-healing capabilities. The bioactive compounds lignin carbon dots and curcumin were incorporated into the wound dressing to provide antibacterial properties against *Staphylococcus aureus* and *Pseudomonas aeruginosa*. Besides, *in vitro* experiments have demonstrated the superior biocompatibility of these wound dressing platforms towards neonatal human dermal fibroblast cell lines (HDFn). Furthermore, these fibrous mats did not exhibit contact and adhesion of microorganisms according to the microbial penetration test. Additionally, the composite fibrous membrane exhibited favorable hydrophilic properties and mechanical strength, making it a promising candidate for multifunctional wound dressings. Finally, it can be combined with regenerative therapies to exploit their photoluminescent and electrical properties as a stimulus for wound healing.

1. Introduction

The skin is the largest organ in the human body and acts as a protective barrier against injuries and infections [1–3]. However, it is also highly vulnerable to damage, which can lead to substantial health and economic burdens [4]. Wound dressings are a usual treatment for skin injuries, but there is a need for improved wound dressings that can promote faster healing and reduce the risk of infection [5–7]. Nanostructured wound dressings explore the advantages of high surface area-to-volume ratio, high porosity, and ability to carry and deliver drug s[8]. Among the most explored nanomaterials for wound dressing applications are the polymer nano- and microfibers, resulting in large fibrous mats that can protect the injured area, absorb the exudates, promote the loading and releasing of therapeutical compounds, and improve gas flow and exchange [9]. Due to their several particularities, nanofibers-based wound dressing are good candidates for multifunctional wound dressing, and novel trend is to combine the conventional properties of a wound dressing to functions like sensing, stimuli-responsiveness, photodynamic therapies, etc.

Solution Blow Spinning (SBS) is an innovative and versatile technique that has gained significant prominence in the preparation of wound dressings [10,11]. The technique utilizes the force of pressurized gas to rapidly stretch and evaporate a polymeric solution jet, forming intricate and finely structured fibers. Unlike electrospinning, SBS does not require high voltage, thus, it simplifies the fiber-forming process and reduce safety concerns. SBS offers several advantages for wound

* Corresponding authors.
E-mail addresses: daniel.correa@embrapa.br (D.S. Correa), rorefice@demet.ufmg.br (R.L. Oréfice).

https://doi.org/10.1016/j.mtcomm.2024.111418
Received 1 October 2024; Received in revised form 24 November 2024; Accepted 22 December 2024
Available online 24 December 2024

dressing applications, including the control of fiber diameter and porosity, allowing the creation of highly porous structures that can promote efficient fluid absorption and moisture management. These porous mats also facilitate gas exchange, crucial for a favorable wound healing environment. Additionally, SBS offers rapid production rates and cost-effectiveness, rendering it an appealing option for large-scale manufacturing of wound dressings [10,12,13].

A variety of synthetic and natural polymers can be used to produce nonwovens wound dressings via SBS technique [2,14]. Among them, poly(lactic acid) (PLA), a biodegradable polyester derived from renewable sources such as corn and sugar cane, has gained substantial attention in the field of wound dressing due to its biocompatibility, mechanical strength, and biodegradability [15,16]. However, PLA presents certain limitations when used in wound dressings. For instance, its relatively slow degradation rate can be a drawback, as it may hinder the dressing's ability to conform to the dynamic wound environment over extended periods [17]. Additionally, PLA can be somewhat hydrophobic, which may affect its moisture-retaining capabilities [1,6,12]. To address these limitations, researchers often combine PLA with other materials or modify its surface properties to improve its overall performance in wound dressings, demonstrating the ongoing efforts to harness the full potential of this biopolymer for effective wound care [18–22].

Curcumin (Cur), a bioactive compound extracted from *Curcuma longa*, has gained significant attention for biomedical applications due to its anti-inflammatory, and antimicrobial properties, which make it a compelling candidate for enhancing wound healing [23,24]. However, curcumin's low bioavailability, poor stability, and rapid degradation can limit its application in wound dressings [25,26]. Strategies to overcome these limitations include developing innovative delivery mechanisms and formulations that enhance curcumin's stability and sustained release at the wound site, offering promising avenues for improving its application in wound care [27–30]. Lignin carbon dots (LCdots) represent an intriguing class of carbon-based nanomaterials with tremendous potential in the biomedical field [31,32]. Derived from lignin, a natural polymer abundant in biomass and agricultural waste, LCdots exhibit remarkable attributes for biomedical applications, including tunable photoluminescence, remarkable fluorescence quantum yields, photostability, dispersibility, and excellent biocompatibility [33]. LCdots can serve as carriers for drug delivery, owing to their ability to encapsulate and release therapeutic agents in a controlled manner [34,35]. Their biocompatibility and low toxicity further enhance their suitability for use in various biomedical contexts, making LCdots a promising platform for multifunctional wound dressings [33,36–40].

In this work, LCdots were produced from hydrothermal synthesis which, in combination with curcumin, were incorporated into PLA fibers produced by SBS technique, as illustrated in Fig. 1. The produced fibrous mats were characterized by Scanning Electron Microscopy (SEM), Fourier Transformed Infrared Spectroscopy (FT-IR), Differential Scanning Microscopy (DSC), Ultraviolet-Visible Spectrophotometer (UV-Vis) and Angle of Contact (CA). Besides, analyzes such as halo of inhibition, cytotoxicity assay and microbial penetration were used to evaluate the ability of these fibrous mats to be applied as skin wound dressings.

2. Experimental

2.1. Materials

Poly(lactic acid) 4060D (Mn = 120,000 g mol^{-1}) was purchased from NatureWorks, USA. Kraft lignin was obtained from Ingevity, USA. Curcumin (Cur) was purchased from Sigma-Aldrich, USA. Chloroform (99.9 %) was purchased from LS Chemicals, while *N,N*-dimethylformamide (DMF) (99.8 %) was purchased from Sigma-Aldrich (Brazil). Microbiological assays, agar and Mueller Hinton broth were obtained from Himedia. Ampicillin sodium salt was purchased from Sigma-Aldrich (Brazil) and tetracycline discs from CASALAB (Brazil).

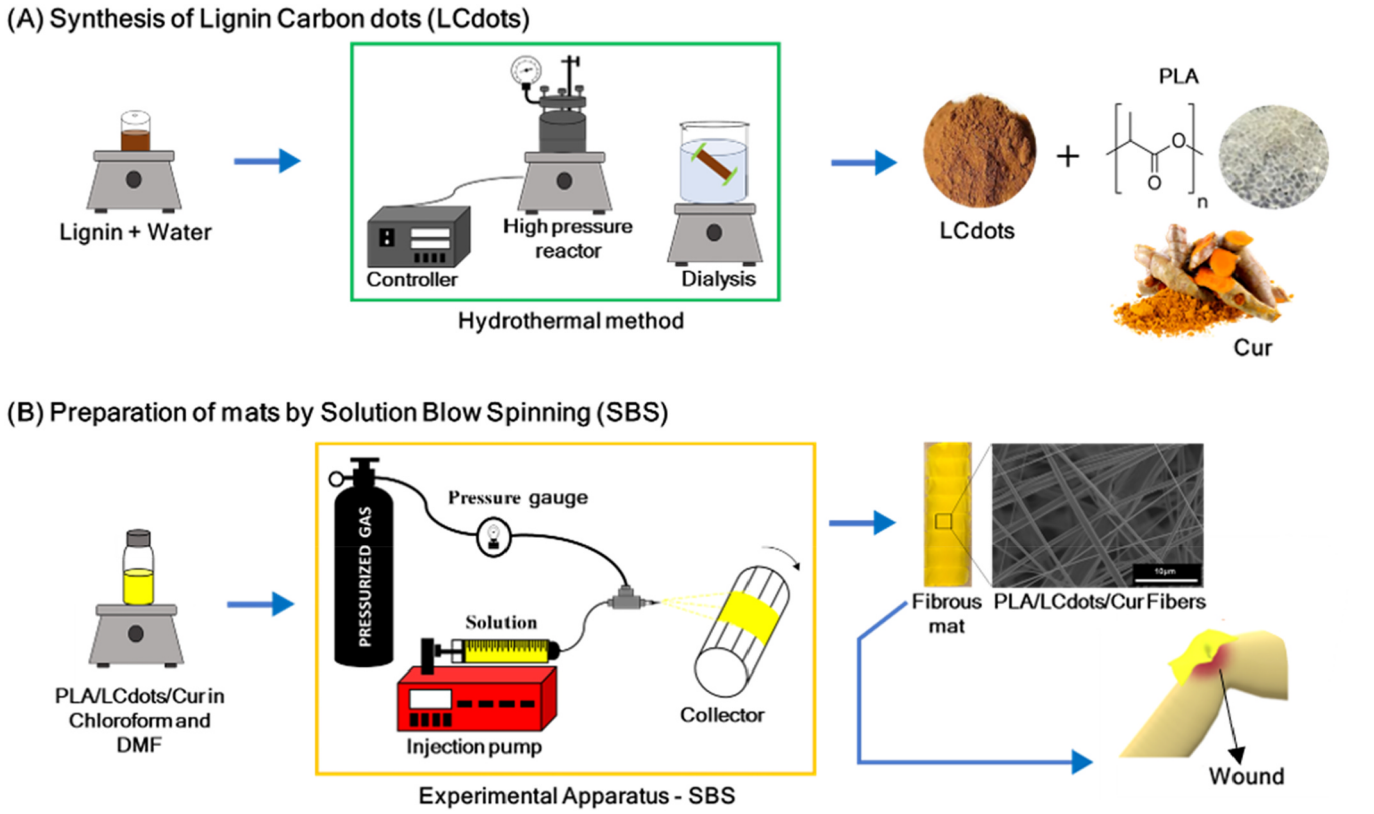

Fig. 1. Schematic representation for the synthesis of LCdots, combined with curcumin and PLA, and b) production of PLA/LCdots/Cur nanofibrous membranes by solution blow spinning for wound dressing applications.

2.2. Synthesis of lignin carbon dots

Lignin carbon dots (LCdots) were synthesized by a hydrothermal method according to the methodology proposed by Liu et. al. [41], Briefly, a 2.5 wt% aqueous solution of lignin placed in a teflon lined stainless steel autoclave was heated up to 180 °C for 5.5 h. The final solution was then filtered through a 0.22 μm syringe filter and dialyzed using a membrane of 2000 Da for 48 h. The concentration of LCdots was determined by freeze-drying a suspension aliquot at −45 °C for 48 h (Liotop L101, Liobrás) resulting in a concentration of 14 ± 0.8 mg of LCdots/g of suspension.

The resulting LCdots were characterized by fluorescence and UV-Vis absorption spectroscopies and electron microscopy. Fluorescence spectra of LCdots suspension were recorded using a Shimadzu RF-5301PC spectrofluorometer with the aid of a quartz cuvette. UV-Vis absorption spectra of the LCdots suspension was collected using a Shimadzu UV-1900 spectrophotometer between 200 and 700 nm. Transmission electron microscopy (TEM) and high-resolution TEM images of the LCdots were obtained using a JEOL JEM2100 LaB6 transmission electron microscope.

2.3. Preparation of fibrous mats (SBS)

PLA mats were produced using the solution blow spinning (SBS) technique. The SBS experimental conditions were optimized, resulting in six different samples (C1 − C6), whose conditions of fabrication are specified in Table S1. The PLA polymer solution (12 % (w/v)) was prepared by using chloroform and N,N-Dimethylformamide (DMF) at a ratio of 4:1 (v/v) as solvent, under magnetic stirring for 15 hours, at room temperature. The spinning was performed using a homemade SBS apparatus consisting of a polymer solution injection system, a compressed air source, a fiber collection system, and a rotating collector. The injection system consisted of a 20 mL glass syringe, a capillary resistant to organic solvents, a 0.5 mm diameter nozzle, and an injection pump. Compressed air was supplied by a Schulz compressor at a pressure of 2 bar. The working distance between the nozzle and the collector was 22 cm. LCdots and curcumin were incorporated to the PLA solution, in the proportion of 2 and 10 wt%, respectively, in relation to the PLA mass. The final samples were named as PLA, PLA/LCdots, PLA/Cur, and PLA/LCdots/Cur.

2.4. Physicochemical characterization of fibrous mats

The mats were characterized in terms of morphology, composition, electrical conductivity, mechanical properties, and the ability to absorb exudates was investigated by the mats swelling capacity, and their hydrophilicity. The morphology was analyzed by Scanning Electron Microscopy using a JEOL JSM-6510 microscope, operating at 5 kV. The samples were coated with a thin layer of gold using a sputter coater (Leica Microsystems EM SCD050). The average fiber diameter was determined using an image processing software (ImageJ 1.45, National Institutes of Health, Bathesda, United States). The fibrous mats compositions were investigated using an infrared spectrometer (PerkinElmer Spectrum 1000 with Spectrum software) equipped with an attenuated total reflection apparatus. The spectra were obtained in the spectral region between 4000 and 400 cm^{-1}, accumulation of 32 scans and a resolution of 2 cm^{-1}.

The electrochemical impedance spectroscopy (EIS) experiment was performed using a PGSTAT30 Autolab potentiostat/galvanostat (Metrohm) controlled by Nova software (version 2.1), using a 5 mM $[Fe(CN)]^{3-/4-}$ solution containing 0.1 M KCl. EIS measurements were performed at open circuit potential (OCP) in the frequency range from 0.1 Hz to 100 kHz, using an voltage amplitude of 10 mV.

The mechanical properties of the mats were evaluated by dynamic-mechanical analysis (DMA) (Q800 equipment), using the mats as specimens with the following dimensions: width 7 of mm, length of 5.5 mm, and average thickness of 0.27 ± 0.06 mm. Tensile tests were performed in uniaxial tension with a ramp of 700 mm min^{-1}, preload force of 0.001 N and deformation amplitude of 0.1 % in the temperature range of 25–30 °C.

The degree of swelling (Sd%) was evaluated by analyzing the PBS buffer absorption capacity. Approximately 6 mg of each fibrous mat (in triplicate) were immersed in vials containing 10 mL of PBS buffer (pH = 7.4). The mass of the specimens was measured after certain periods of time. The degree of swelling (Sd%) was then calculated from Eq. (1) [42,43]

$$S_{d(\%)} = \frac{w_t - w_0}{w_0} \times 100 \quad (1)$$

where w_0 and w_t are the initial mass of the sample and the mass of the sample at time t, respectively. The dynamic contact angle of the wound dressings was evaluated at 25 °C using a contact angle goniometer (model CAM 101, KSV Instruments) equipped with a charge-coupled device camera (KGV-5000). 5 μL drops of deionized water (approximately 5 μL) were placed on the surface of the fibrous mats specimens (1 cm × 1 cm), and measurements were taken from images of the angle formed between the drop and the surface of fibrous mats, using the KSV CAM 2008 software. Experimental data originated from mechanical tests and contact angle assay were compared with One-Way ANOVA test and group means were compared with Tukey test, both with a 0.05 significance level.

2.5. Cost estimation of fibrous mats

The PLA, PLA/LCdots, PLA/Cur and PLA/LCdots/Cur fabrication process was mapped to estimate the cost of the fibrous mats used as a dressing. Infrastructure, equipment, maintenance, and disposal cost were disregarded, as presented in Table S2.

2.6. Encapsulation efficiency and In Vitro controlled release assay

The encapsulation efficiencies (EE) of LCdots and Curcumin into the PLA fibrous mats were determined following the methodology previously reported by [44,45] using Eq. (2).

$$EE(\%) = \frac{Amount\ of\ compound\ measured}{Theorical\ amount\ of\ compound} \times 100 \quad (2)$$

Specimens of 6 mg of PLA, PLA/LCdots, PLA/Cur, and PLA/LCdots/Cur were dissolved in 10 mL of a chloroform and DMF solution (4:1 v/v) for 12 h. Next, the absorbance at 280 nm and 420 nm was measured using a UV-Vis spectrophotometer (Shimadzu UV 1100), and the values were compared to previously built calibration curves. For the calibration curves, different amounts of LCdots and Curcumin were dissolved in chloroform and DMF (4:1 v/v) and the absorbances at 280 nm and 420 nm were recorded. The calibration curve, the respective equation and the values of linear regression can be seen in Figure S2. The measurements of the content of Cur and LCdots in the samples were carried out in triplicate.

The *in vitro* Cur and LCdots release assay were performed in a PBS solution (0.1 mol L^{-1}, pH 7.4), aiming to simulate physiological conditions of blood plasma or exudates present in skin wounds [46]. Tween-80 (1.0 v/v%) was mixed with the PBS solution, aiming to minimize degradation effects of Curcumin [47]. Specimens of 6 mg of the PLA, PLA/LCdots, PLA/Cur, and PLA/LCdots/Cur were immersed into 20 mL of the PBS/Tween-80 solution and incubated at 37 °C, under gentle agitation, and protected from light. The absorbances at 280 and 420 nm were measured using UV-Vis spectroscopy technique at a specific time intervals (which are described in Table S3), achieving 216 hours. The experiments were carried out in triplicate for each sample.

2.7. Antibacterial activity experiments

Staphylococcus aureus (ATCC 25923) and *Pseudomonas aeruginosa* (ATCC 27853) were stored as frozen glycerol stocks. *S. aureus* was grown on tryptic soy agar (TSA) with 6 g/L yeast extract, while *P. aeruginosa* was grown on nutrient agar (NA). After incubation at 37 °C, single colonies were suspended in Müeller Hinton broth (MHB) and batch-cultured for 24 h at 37 °C and 150 rpm. Cultures were diluted in fresh MHB to 5×10^8 CFU/mL to ensure exponential growth. The antimicrobial activity of fibrous mats was tested using the disk diffusion method with MHB-agar plates streaked with bacterial suspensions adjusted to 0.5 McFarland (10^8 CFU/mL). Filter paper disks with ampicillin (10 μg) and tetracycline (30 μg) served as controls. Plates were incubated at 37 °C for 24 h. For the microbial penetration test, sterile test tubes with 15 mL of MHB were sealed with fibrous membranes (2 cm × 2 cm) or parafilm (negative control), while the positive control tube remained open. After 10 days at room temperature, 20 μL of the medium from each tube was applied to filter paper discs placed on agar plates to assess bacterial growth. The plates were incubated at 36 °C for 24 h to verify the inhibition of bacterial growth from the mats, as illustrated in Figure S1[48,49].

2.8. In Vitro cytotoxicity test

Cytotoxicity experiments were performed using the Human Dermal Fibroblast neonatal (HDFn) cell line, cultured in DMEM supplemented with 10 % FBS under standard conditions (37 ºC, 5 % CO_2). Cells were maintained and subcultured as needed, following standard protocols [50–52]. The MTT assay was employed to assess the cytotoxicity of PLA mats by evaluating cell metabolic activity. Membrane extracts were prepared by incubating UV-sterilized mat samples (1 cm^2 each) in DMEM supplemented with 10 % FBS for 24 h. HDFn cells (1×10^4 cells/well) were exposed to these extracts for 24 or 48 h. Control groups were incubated with DMEM 10 % FBS without mat exposure. After exposure, the MTT assay was conducted by adding MTT solution (0.5 mg/mL in DMEM) to each well, followed by a 3 h incubation. Formazan crystals formed were dissolved in DMSO, and absorbance was measured at 570 nm and 690 nm. Relative metabolic activity was normalized to control group values (set at 100 %). Results (mean ± SD, n = 6) were analyzed using One-Way ANOVA and Tukey's test with a significance level of 0.05.

3. Results and discussions

3.1. Morphology and characterization of LCdots

TEM analysis (Fig. 2A) confirmed the LCdots synthesis was successful, which are the darkest dots in the image. A high-resolution TEM image of an individual LCdots revealed the lattice spacing of 2.4 nm in the crystalline plane (Fig. 2A). The distribution of LCdots diameters, measured from Fig. 2B, showed a mean diameter of 2.4 ± 0.5 nm (Fig. 2B), similar to the work reported by Liu et al., with carbon dots displayed an average diameter of 3.4 nm [53]. Fluorescence spectroscopy (Fig. 2C) showed that the luminescent intensity of the LCdots decreased as the excitation wavelength increased from 300 to 400 nm. The strongest fluorescence emission band was observed at around 390 nm, under 300 nm excitation wavelength, similar to the results reported by Nie et al [54]. The UV-Vis absorption spectrum of LCdots (Fig. 2D) shows a band centered at approximately 280 nm, which may be associated with electronic transitions in the C═O or aromatic C═C bonds [34].

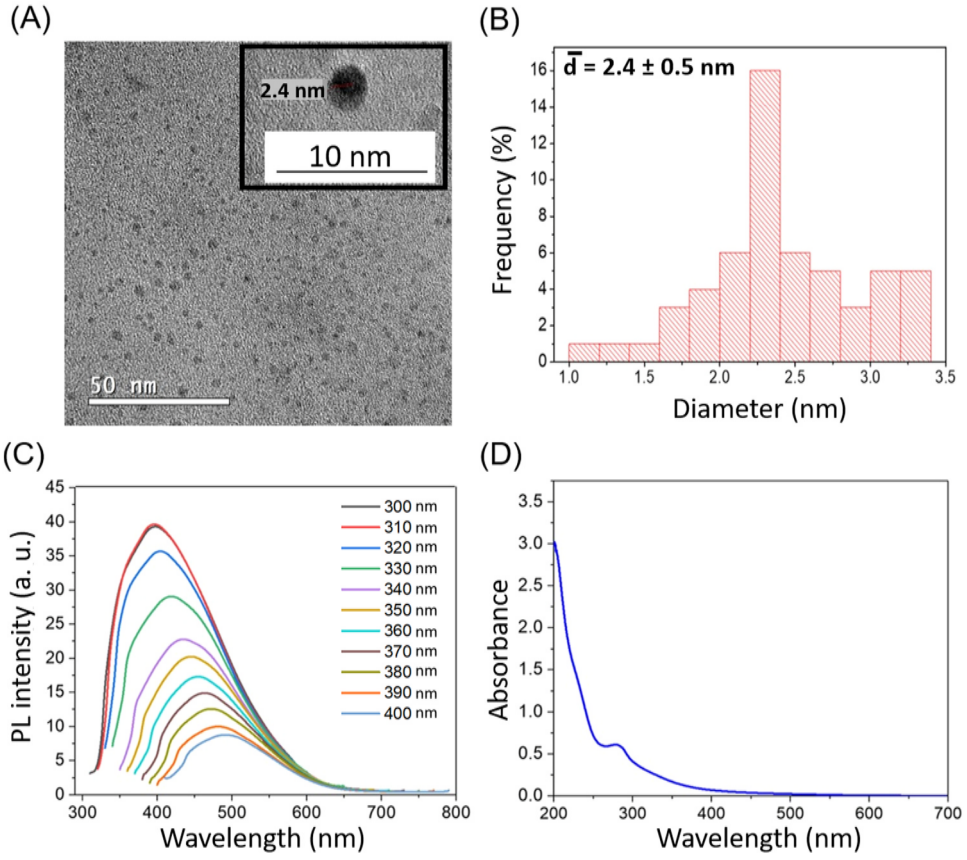

Fig. 2. (A) TEM image of LCdots. The inset shows a High-Resolution TEM image of an individual LCdot. (B) histogram of size distribution of LCdots. (C) PL spectra of LCdots under different excitation wavelengths (from 300 up to 400 nm), (D) UV–vis absorption spectrum of LCdots.

3.2. Physicochemical characterization

Fig. 3 depicts the micrographs of the PLA, PLA/LCdots, PLA/Cur, and PLA/LCdots/Cur fibrous mats. It is possible to observe a network of submicrometric fibers characterized by predominantly continuous cylindrical morphology, which exhibit uniformity and are randomly distributed. A noteworthy reduction in fiber diameter was observed as consequence of the incorporation of LCdots and curcumin to the

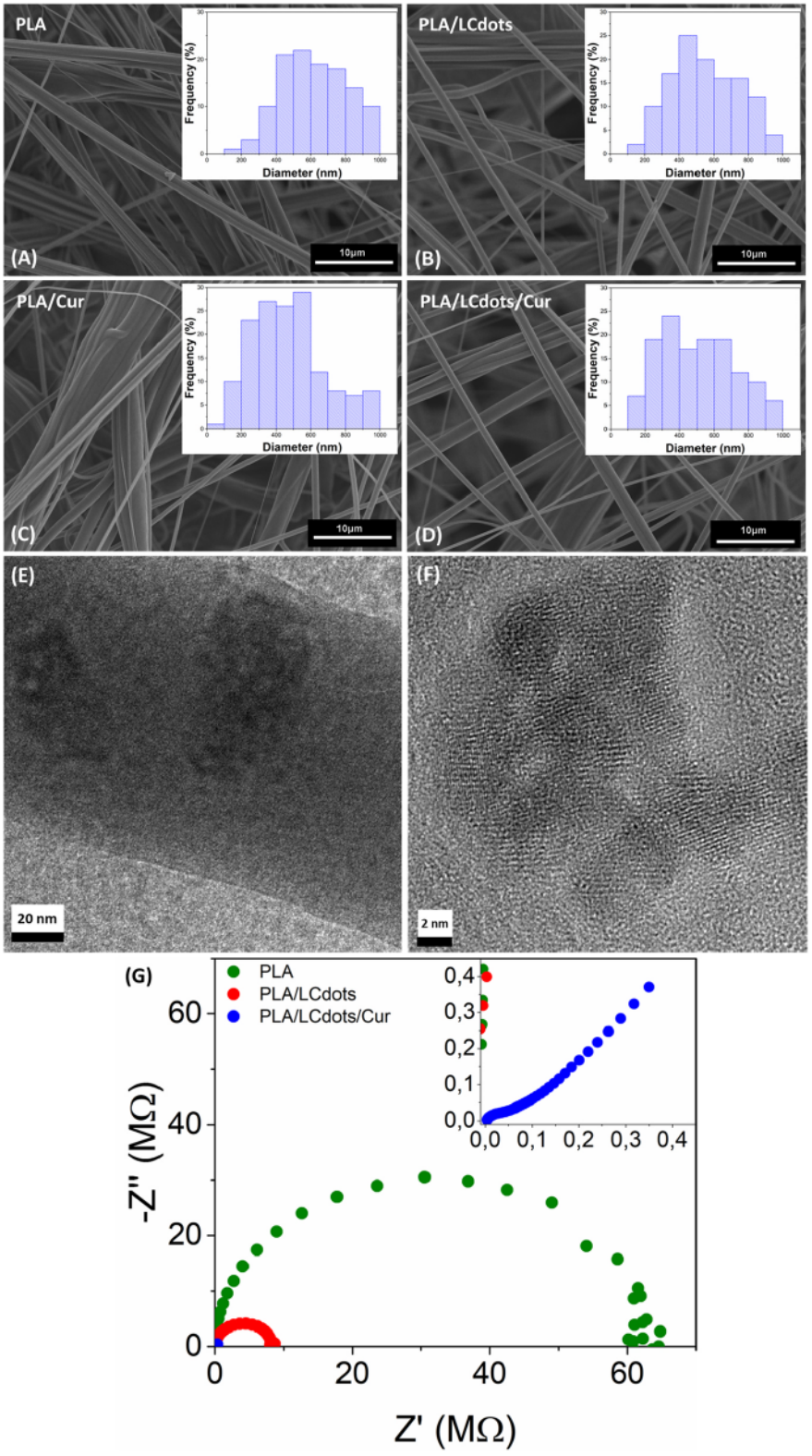

Fig. 3. SEM micrographs and histogram of fiber diameter distribution of (A) PLA, (B) PLA/LCdots, (C) PLA/Cur and (D) PLA/LCdots/Cur mats. TEM image of (E) LCdots in the fiber, and (F) high resolution TEM image of LCdots in the fiber with the in-plane lattice spacing. Nyquist plots of (G) EIS of PLA, PLA/LCdots, and PLA/LCdots/Cur mats in a 5 mM $[Fe(CN)^6]^{3-/4-}$ solution with 0.1 M KCl.

formulation, (Fig. 3B). Specifically, PLA/LCdots and PLA/Cur exhibit average diameters of 551 ± 18 nm and 468 ± 17 nm, respectively. This reduction is in contrast to the PLA-only composition, which exhibited mean diameter of 619 ± 17 nm. This phenomenon indicates that the incorporation of LCdots and curcumin into the PLA solution results in the formation of thinner fibers during the spinning process, as previously documented by Teodoro et. al. [6], in the case of curcumin-based fibers. As expected, it was verified that the combination of both LCdots and curcumin in the PLA/LCdots/Cur composite yielded fibers with smaller diameters of 512 ± 19 nm (Fig. 3D). Fig. 3E shows the TEM analysis of a fiber obtained by Solution Blow Spinning containing the LCdots, from which it is possible to observe the incorporation of LCdots in the PLA fiber. By the high-resolution TEM micrograph in Fig. 3F it is possible to observe the lattice spacing in the crystalline plane of the LCdots.

Adding LCdots and Curcumin into PLA solution decreased the solution viscosities. Specifically, the viscosities of PLA, PLA/LCdots, PLA/Cur, and PLA/LCdots/Cur were 68, 65, 57, and 52 cP, respectively. This reduction in viscosities of polymer solutions containing the bioactive LCdots and curcumin also helped the formation of fibers of smaller diameters.

3.2.1. Electrochemical impedance spectroscopy (EIS)

In order to investigate the potential of the wound dressings to be integrated into electro-stimulated therapies, the electron transfer properties of the fibrous mats were evaluated by EIS. Fig. 3G exhibits the Faradaic impedance spectra, in which the diameter of the semicircle is associated with the electron transfer resistance (R_{ct}) of a Randle's equivalent circuit [55] R_{ct} values were 65, 8.0 and 0.5 MΩ for PLA, PLA/LCdots and PLA/LCdots/Cur, respectively, indicating a substantial decrease as a consequence of LCdots and Curcumin incorporation. Furthermore, the results obtained for PLA/LCdots/Cur mats consolidate a synergistic effect between the bioactives LCdots and Curcumin, indicating that this material can effectively promote faster electron transfer between electrode interface [56–59].

3.2.2. Fourier transform infrared spectroscopy (FTIR)

Figure S3A presents the FTIR spectra of PLA, lignin carbon dots (LCdots) and curcumin (Cur) starting materials. It is possible to observe, for PLA, the characteristic bands of this polymer in the regions between 2996 and 2946 cm^{-1}, which correspond to the -CH stretching, at 1744 cm^{-1}, a band associated with a carbonyl vibration (C═O), stretching of different C−O bonds at 1125 cm^{-1} and C−C stretching at 1082, 1040, and 869 cm^{-1}[60].

In Figure S3A, it is observed for the spectrum of curcumin the region of absorption bands around 3510 cm^{-1}, which corresponds to the elongation of the hydroxyl functional groups, and at 1603 and 1625 cm^{-1} the stretching vibration of the C═C bond. The band at 1507 cm^{-1} is attributed to the stretching of -O aromatic and -O-R aromatic groups. Besides, at 1155 cm^{-1}, distinct stretching vibrations for CH_3, CH_3 methoxy aromatic groups are observed. Furthermore, the peak at 1272 cm^{-1} is ascribed to phenolic C-O stretching vibrations [26].

LCdots present bands related to lignin spectrum, including in the regions between 3400 and 3460 cm^{-1}, referring to axial deformations associated with hydroxyl groups (OH), at 2982 and 2896 cm^{-1}, referring to the axial deformations C-H of aliphatic chains CH_2 and CH_3, and at 1620 and 1510 cm^{-1}, referring to the various vibrations of the skeleton of aromatic rings [36].

In Figure S3B it is observed that the starting materials LCdots and curcumin were incorporated into the PLA solution. Specifically, the peak at 1678 cm^{-1} is indicative of the vibrations associated with the aromatic rings skeleton for the LCdots. Besides, in the region spanning from 1628 and 1500 cm^{-1}, stretching vibrations of the C═C bond and the aromatic -O and aromatic -O-R stretching vibrations for curcumin are observed.

3.2.3. Mechanical test

Values of elastic modulus, tensile strength and elongation-at-break of PLA, PLA/LCdots, PLA/Cur and PLA/LCdots/Cur mats were obtained from stress-strain curves and are represented in Figure S3C, S3D and S3F, respectively. The results were compared with pure PLA mats, and all samples described a typical stress vs strain curve, where first stages correspond to linear elastic behavior, followed by plastic nonlinear region.

From the Tukey test applied to the stress-strain curves, it was possible to confirm a statistically significant difference in the increase of elastic modulus values when LCdots and Cur are incorporated into the PLA polymeric solution. In the work of Liu et. al., this increase was also reported as the concentration of carbon dots incorporated into polyurethane and polyacrylonitrile nanofibers increased [53]. Similarly to Pankongadisak et al., who reported in their work that as the concentration of curcumin increases in PLLA fiber mats, an increase in the mechanical properties of these materials is observed [61]. It is also observed that the mats containing LCdots in their composition present higher elastic modulus values (Figure S3C). However, a slight decrease was observed for the PLA/LCdots mat, not statistically significant, and a more significant decrease for PLA/Cur and PLA/LCdots/Cur mats in the tensile strength limit values (Figure S3D). Regarding elongation, a statistically significant reduction was also observed in the elongation values for PLA/LCdots, PLA/Cur and PLA/LCdots/Cur mats in relation to pure PLA mat, however, it was noted that there was no significant difference in reducing the elongation between the PLA/Cur and PLA/LCdots/Cur mats (Figure S3E). In general, the mechanical properties of the as-developed wound dressings are similar to other fiber-based materials reported in the literature [1,62,63].

3.2.4. Contact angle and swelling degree ($S_{d\%}$)

Surface hydrophobicity is typically assessed by quantifying the static contact angle of a liquid droplet on a specific sample surface. A higher contact angle indicates an increased degree of surface hydrophobicity. Assessing the hydrophilic nature of fibrous mats holds significant importance, as it serves as a predictive tool to guide the potential applications of these materials [64]. For example, the surface hydrophilicity of spun mats plays a crucial role in the development of wound dressings for the treatment of skin wounds. It is directly associated with aspects such as cellular adhesion, proliferation of microorganisms, and absorption capacity for skin exudates [65]. This underscores the relevance of this assessment for tailoring these materials to meet the specific requirements of biomedical applications. The contact angles between the water droplet and the surface of mats are shown in the Fig. 4A.

Fig. 4: (A) Values of contact angles after the 1st second of contact between the drop of water and the surface of mats (A), and (B) Swelling degree of PLA, PLA/LCdots, PLA /Cur and PLA/LCdots/Cur mats.

The swelling capabilities of PLA, PLA/LCdots, PLA/Cur and PLA/LCdots/Cur mats were studied, as shown in Fig. 4B. It can be observed that mats containing LCdots in their composition (PLA/LCdots and PLA/LCdots/Cur) showed a higher degree of swelling of 733 and 747 %, respectively, reaching equilibrium after approximately 24 h later, while PLA and PLA/Cur mats presented Sd% values of 716 and 674.09 %, respectively. The value obtained for the pure PLA mat was similar to the value reported by Grizzo et. al [1]. This indicates that the PLA/LCdots and PLA/LCdots/Cur mats possess better water absorption capabilities than the other materials for times longer than 24 h. This result is consistent with those obtained in the contact angle experiment (Fig. 4A), in which the PLA/LCdots and PLA/LCdots/Cur mats presented lower contact angles, that is, greater hydrophilicity [71].

3.3. Encapsulation efficiency and antibiotic In Vitro release assay

Actual content of Cur and LCdots into the fibers were evaluated by studying the encapsulation efficiency (%EE), which values are displayed in Table 1. The lower value calculated for LCdots encapsulation in the sample PLA/LCdots/Cur suggests interference from the presence of Cur, since this component is majority in the formulation. The co-release of

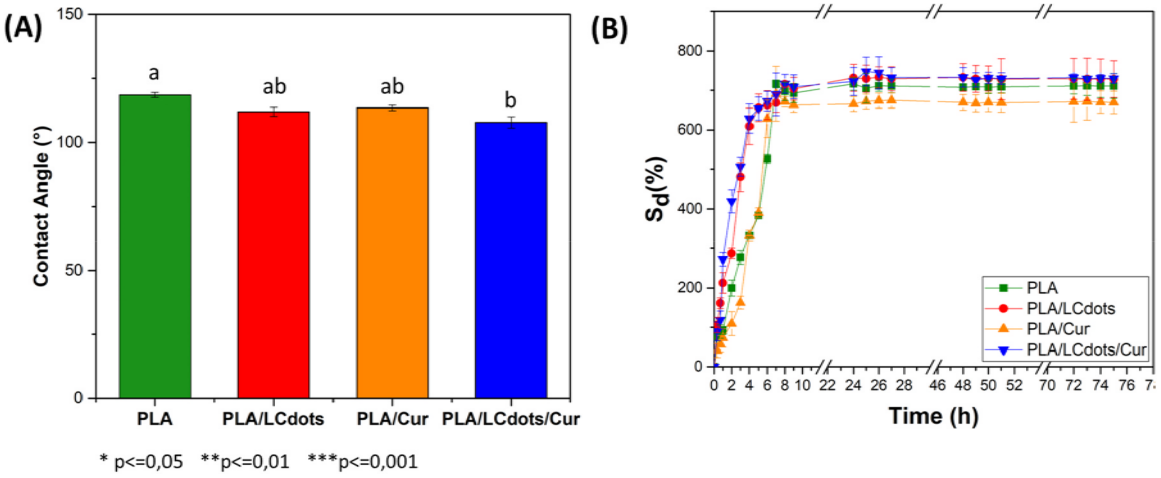

Fig. 4. A shows the decrease of contact angles for the fibrous mats containing LCdots and Curcumin. Initially, a high contact angle of 118.5° ± 1.5° is observed for PLA, which is expected due to its hydrophobic nature of this polymer [66,67]. When LCdots and curcumin are incorporated separately, a slight decrease in the contact angles was observed, whose values corresponds to 111.9° ± 1.5° and 113.5° ± 1.6°, respectively. According Tukey test, these values are not statistically significant when compared to the PLA fibrous mat. When both components are incorporated, a more prominent decrease in the contact angle is verified, reaching the value of 107.8° ± 2.0°, which represents a decrease of approximately 10 % in relation to the mat composed only of PLA, which according Tukey test, presents a significant difference in its values. The reduction in contact angle values as consequence of the incorporation of LCdots and Cur (separately or together) can be explained due to the presence of the hydrophilic functional groups of carbon dots for the LCdots, as reported in the literature [68–70].

Table 1
The constants and coefficient of correlation (R^2) for Korsmeyer-Peppas model applied for all wound dressings.

Analyzed compounds	EE (%)	Korsmeyer-Peppas Model		
		n	k (h^{-1})	R^2
Cur in PLA/Cur	74.2 ± 3	0.28	0.069	0.99
Cur in PLA/Cur/ LCdots	72.0 ± 1	0.32	0.070	0.98
LCdots in PLA/ LCdots	77.6 ± 5	0.09	0.030	0.86
LCdots in PLA/Cur/ LCdots	58.8 ± 1	0.07	0.032	0.92

Cur and LCdots was studied by the release profiles described by each component separately, during a period of 144 h (equivalent to 6 days). The correlation between the cumulative release percentage and the time are shown in Fig. 5A. Upon examining the curcumin released from samples PLA/Cur and PLA/LCdots/Cur, it is observed that the total content was released during the first 10 hours (Fig. 5B), immediately after the burst phases. In contrast, the release profiles described by LCdots is characterized by values of cumulative release in a range of 30 – 40 %, in such a way that 29 % of the LCdots content was released in the first hour. After 10 h, the monitored content of LCdots in the analyzed media followed a cumulative release approximately constant until the end of the assay. The cumulative release curves for PLA/LCdots/Cur in relation to Cur and to LCdots indicate that one component was minimally affected by the presence of the other in the formulation.

The mechanisms involved in the release process were further investigated using the Kormeyer-Peppas kinetic models [72,73], which can assist to infer the phenomena involved in the Cur and LCdots release from the PLA SB-spun wound dressings. The resultant release kinetic parameters are summarized in Table 1. Numerous studies in literature indicate that controlled release results are a consequence of phenomena like the solubilization of the surface content of the drug (leaching), characterized by the typical bursts. Additionally, the release of encapsulated compound is typically governed by diffusional processes or potential erosions within the polymer structures. Satisfactory agreements with Korsmeyer-Peppas model were verified, mainly for PLA/Cur (R^2 = 0.99). The values of $n < 0.5$ found for all the samples indicated the predominance of a typical Fickian diffusion mechanism, which is a consequence of concentration gradient between the carrier (nanofibers) and the solution media. Fig. 5C displays the FESEM image of a representative region of the neat PLA fibers after the controlled release experiment. It is possible to observe surface erosion of the fiber, which can be correlated with the leaching of compounds from the fibers [6]. This erosion pattern was consistent across all samples, as can be observed in Figure S4.

3.4. Biological characterization

3.4.1. Disk diffusion method

S. aureus and P. aeruginosa stand out as some of the most prevalent pathogenic bacteria causing chronic wound-related infections [74]. The common wound dressings currently available in the market are usually films, sponges, and foams, however multifunctional wound dressing materials are urgent due to the evolvement of multi-resistant strains [75]. In this context, biohybrid nanofibers can outperform classical drug delivery systems [76]. To evaluate the hypothesize that PLA mats containing lignin carbon dots (LCdots) and curcumin (Cur) can be an optimal dressing local delivery at the wounded site, their antimicrobial activity was tested against S. aureus and P. aeruginosa by the disk diffusion method.

As shown in Figs. 6A and 6B, no inhibition zones were observed around the specimens. Nevertheless, all samples (excluding the control sample based on neat PLA) enhibited the ability to inhibit bacterial growth upon contact, as confirmed for both bacteria strains tested. Moreover, the presence of aromatic rings of both LCdots and curcumin, as observed in the FTIR spectrum in Figure S3, when incorporating the active ingredients into the polymeric solution, can interact to yield the formation of physical or chemical interactions with the PLA polymeric structure [60,77]. This interaction may hinder the diffusion of active compounds in the medium, consequently leading to the absence of inhibition zone [78]. Specifically, the antibacterial activity of these materials can be attributed to the presence of curcumin and lignin in the fibrous mats. Curcumin is known to target the cell wall, binding to peptidoglycan, which is essential for bacterial viability [79,80]. On the other hand, the phenolic groups present in lignin are responsible for its antibacterial effect through oxidative stress and the ability to produce reactive oxygen species, resulting in the cell membrane destabilization. Furthermore, lignin carbon dots are very sensitive to pH due to the ionization of surface functional groups (in particular, carboxylic acid groups), demonstrate lower toxicity and better biocompatibility, and

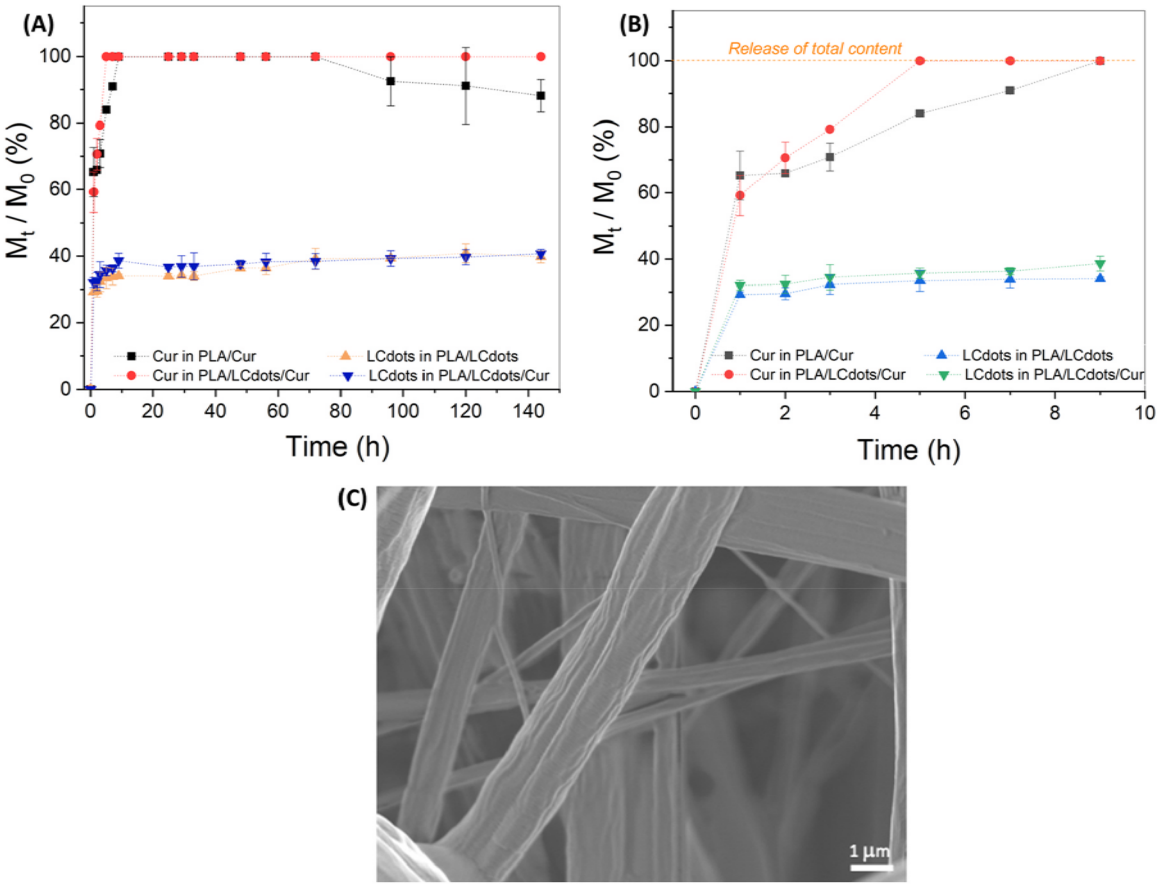

Fig. 5. (A) Cur and LCdots release profiles of the samples PLA/Cur, PLA/LCdots/Cur and PLA/LCdots during 144 h of assay and (B) details of the first 10 h of assay. (C) FESEM micrography of a representative region of a sample analyzed after 144h-assay.

have many hydrophilic surface functional groups so that they can disperse easily in aqueous media without additional surface modification [35,81–84]. In summary, these findings are promising for the prospects of utilizing polymeric nanofibrous mats combined with bioactive compounds for wound dressing applications.

3.4.2. *Microbial penetration tests*

An additional antimicrobial test was carried out to assess the capability of fibrous mats produced by the SBS technique to hinder the penetration of external bacteria present in the environment under these mats. Preventing such penetration is crucial as it could compromise the wound healing process. In Fig. 6C, test tubes filled with MHB medium are observed, with the positive control (C+) not sealed, while the negative control (C-) was sealed with parafilm and the others were sealed with pieces of fibrous mats PLA, PLA/LCdots, PLA/Cur and PLA/LCdots/Cur, respectively. It is possible to observe that only in the tube corresponding to the positive control there was growth of colonies, which was confirmed after the inoculation of 20 µL of the C+ content placed on the agar plate, as seen in Fig. 6D. For the other tubes, sealed with parafilm (C-) and with the fibrous mats (PLA, PLA/LCdots, PLA/Cur and PLA/LCdots/Cur) no variation in the turbidity of the MBH neither evidence of growth of microorganisms was verified, as shown in Fig. 6C. These results were also observed in Fig. 6D, where the filter papers referring to each sample are observed without the growth of microorganisms. In summary, the results presented by Figs. 6C and 6D corroborate the inhibition by contact in the inhibition halo tests shown in Figs. 6A and 6B, indicating that the low hydrophilic character of PLA may have contributed to prevent the contact and adhesion of microorganisms in the fibrous mats. Also, the low solubility of curcumin may not have allowed the formation of inhibition halos, but an inhibition by contact was observed.

3.4.3. *Cytotoxicity studies*

For assessing PLA fibrous mat potential cytotoxicity, MTT assay was performed after 24 h and 48 h of human fibroblasts exposure to fibrous mat extracts. There were four types of extracts derived, namely PLA, PLA/LCdots, PLA/Cur or PLA/LCdots/Cur, with the addition of a control group, not exposed to any mats (DMEM 10 % SFB only). Cytotoxicity MTT-assay results (Figs. 6E and 6F) demonstrated that the variations of compositions of PLA fibrous mat were not capable of modulating fibroblast metabolic activity, even after 48 h of extract exposure. Tukey Test comparison showed no statistically significant difference among groups, meaning that exposure to membrane extracts did not have a cytotoxic effect on cells, when compared to control. According to ISO 10993–5:2009 which describes test methods to assess the *in vitro* cytotoxicity of medical devices or extracts of a device, a material is only considered to be cytotoxic when there is a reduction in cell viability greater than 30 % compared to control. Therefore, these results indicate that PLA fibrous mats, even when associated with lignin Carbon dots (LCdots) and curcumin (Cur), did not cause cytotoxic effects on human fibroblast, suggesting cytocompatibility, being a promising alternative to wound dressing.

4. Conclusion

We have successfully developed a multifunctional wound dressing by utilizing biodegradable polymer (PLA), LCdots, and Curcumin through an efficient and cost-effective process based on the SBS technique. Our results indicate that the incorporation of LCdots and Curcumin did not induce significant structural changes in the fibrous mat, while

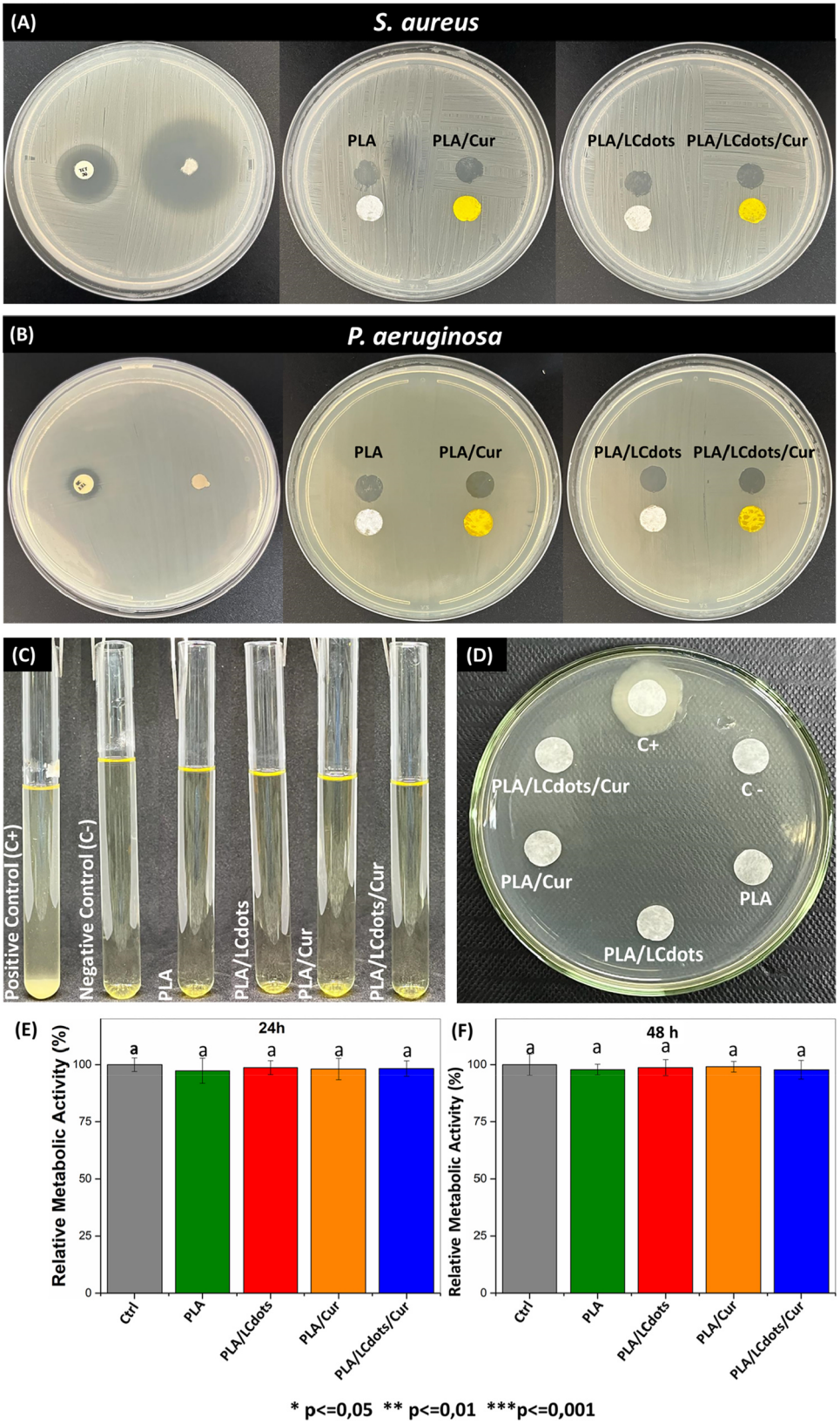

Fig. 6. Antibacterial efficiency validated via disk diffusion assay for (A) S. aureus and (B) P. aeruginosa. Antibiotics controls were included: for S. aureus inhibition zone diameter of 29.6 ± 0.5 and 22.3 ± 2.3 mm for ampicillin and tetracycline, respectively, while for P. aeruginosa inhibition zone diameter of 11.5 ± 2.1 mm for tetracycline. (C) Microbial penetration tests: growth/no growth of microorganisms in tests tubes sealed with PLA, PLA/LCdots, PLA/Cur and PLA/LCdots/Cur mats, and the respective negative (C−) and positive (C+) controls and (D) confirmation of the visual verification by inoculation of 20 μL of each tube matter in agar plates, followed by incubation. Graphs of relative metabolic activity of fibroblasts analyzed with MTT-assay, after 24 h (E) or 48 h (F) of extract exposure (results represented by mean ± standard deviation).

presenting antimicrobial properties against *S. aureus* and *P. aeruginosa*, as demonstrated by the disk diffusion and microbial penetration tests. Furthermore, the fibrous mats resisted bacterial adhesion and exhibited favorable hydrophilic properties and mechanical strength. Cytotoxicity studies revealed no adverse effects on the tested cells, suggesting biocompatibility. However, further *in vivo* studies was required to confirm the safety and efficacy of the developed wound dressing under physiological conditions. Moreover, the inclusion of curcumin and lignin carbon dots opens additional avenues for innovation: curcumin could serve as a colorimetric pH indicator during wound healing, while lignin's conductive properties hold promise for wearable sensor applications. These features could transform the wound dressing into a multifunctional diagnostic and therapeutic platform. In summary, while additional studies are necessary to validate the clinical utility of the developed wound dressing, our findings pave the way for developing sustainable multifunctional wound dressings for advanced wound care.

CRediT authorship contribution statement

Danilo Santos: Writing – review & editing, Visualization, Validation, Methodology, Investigation, Data curation, Conceptualization. **Dr. Kelcilene Teodoro:** Writing – review & editing, Writing – original draft, Visualization, Validation, Methodology, Investigation, Data curation, Conceptualization. **Patrícia Rossi:** Writing – review & editing, Writing – original draft, Visualization, Validation, Project administration, Methodology, Investigation, Data curation, Conceptualization. **Daniel Souza Correa:** Writing – review & editing, Supervision, Conceptualization, Project administration, Resources. **Natalia Inada:** Writing – review & editing, Visualization, Validation, Methodology, Investigation, Data curation. **Camila Costa:** Methodology, Investigation, Writing – review & editing. **Crisiane Maragon:** Writing – review & editing, Visualization, Validation, Methodology, Data curation. **Rodrigo Orefice:** Writing – review & editing, Writing – original draft, Supervision, Conceptualization.

Declaration of Competing Interest

The authors declare that they have no known competing financial interests or personal relationships that could have appeared to influence the work reported in this paper.

Acknowledgements

The authors thank the Conselho Nacional de Desenvolvimento Científico e Tecnológico (CNPq) (140681/2020-5), Fundação de Amparo à Pesquisa do Estado de São Paulo (FAPESP) (2023/13428-0, 2013/07276-1 and 2018/22214-6), Coordenação de Aperfeiçoamento de Pessoal de Nível Superior (CAPES), Brazil, and Rede Agronano-EMBRAPA from Brazil for financial support and infrastructure.

Appendix A. Supporting information

Supplementary data associated with this article can be found in the online version at doi:10.1016/j.mtcomm.2024.111418.

Data Availability

Data will be made available on request.

References

[1] A. Grizzo, D.M. dos Santos, V.P.V. da Costa, R.G. Lopes, N.M. Inada, D.S. Correa, S. P. Campana-Filho, Multifunctional bilayer membranes composed of poly(lactic acid), beta-chitin whiskers and silver nanoparticles for wound dressing applications, Int J. Biol. Macromol. 251 (2023), https://doi.org/10.1016/j.ijbiomac.2023.126314.

[2] D.M. Dos Santos, D.S. Correa, E.S. Medeiros, J.E. Oliveira, L.H.C. Mattoso, Advances in functional polymer nanofibers: from spinning fabrication techniques to recent biomedical applications, ACS Appl. Mater. Interfaces 12 (2020) 45673–45701, https://doi.org/10.1021/acsami.0c12410.

[3] A. Memic, T. Abudula, H.S. Mohammed, K. Joshi Navare, T. Colombani, S. A. Bencherif, Latest progress in electrospun nanofibers for wound healing applications, ACS Appl. Bio Mater. 2 (2019) 952–969, https://doi.org/10.1021/acsabm.8b00637.

[4] S. Sharifi, M.J. Hajipour, L. Gould, M. Mahmoudi, Nanomedicine in healing chronic wounds: opportunities and challenges, Mol. Pharm. 18 (2021) 550–575, https://doi.org/10.1021/acs.molpharmaceut.0c00346.

[5] R.S. Ambekar, B. Kandasubramanian, Advancements in nanofibers for wound dressing: a review, Eur. Polym. J. 117 (2019) 304–336, https://doi.org/10.1016/j.eurpolymj.2019.05.020.

[6] K.B.R. Teodoro, A.D. Alvarenga, L.F. Rocha Oliveira, P.A. Marques Chagas, R. G. Lopes, R. da, S. Andre, L.A. Mercante, F. Alves, M.D. Stringasci, H.H. Buzza, N. M. Inada, D.S. Correa, Fast fabrication of multifunctional PCL/curcumin nanofibrous membranes for wound dressings, ACS Appl. Bio Mater. 6 (2023) 2325–2337, https://doi.org/10.1021/acsabm.3c00177.

[7] J.L. Daristotle, L.W. Lau, M. Erdi, J. Hunter, A. Djoum, P. Srinivasan, X. Wu, M. Basu, O.B. Ayyub, A.D. Sandler, P. Kofinas, Sprayable and biodegradable, intrinsically adhesive wound dressing with antimicrobial properties, Bioeng. Transl. Med 5 (2020), https://doi.org/10.1002/btm2.10149.

[8] M. Akrami-Hasan-Kohal, L. Tayebi, M. Ghorbani, Curcumin-loaded naturally-based nanofibers as active wound dressing mats: Morphology, drug release, cell proliferation, and cell adhesion studies, N. J. Chem. 44 (2020) 10343–10351, https://doi.org/10.1039/d0nj01594f.

[9] K.B.R. Teodoro, D.M. Santos, C.A.S. Ballesteros, P.A.M. Chagas, V.P.V. Costa, R. Schneider, D.S. Correa, Multifunctional Wound Dressings Based on Electrospun Nanofibers. in: Electrospun Nanofibers, Springer International Publishing, Cham, 2022, pp. 297–329, https://doi.org/10.1007/978-3-030-99958-2_11.

[10] E.S. Medeiros, G.M. Glenn, A.P. Klamczynski, W.J. Orts, L.H.C. Mattoso, Solution blow spinning: a new method to produce micro- and nanofibers from polymer solutions, J. Appl. Polym. Sci. 113 (2009) 2322–2330, https://doi.org/10.1002/app.30275.

[11] A.D. Juncos Bombin, N.J. Dunne, H.O. McCarthy, Electrospinning of natural polymers for the production of nanofibres for wound healing applications, Mater. Sci. Eng. C. 114 (2020), https://doi.org/10.1016/j.msec.2020.110994.

[12] M. Wojasiński, M. Pilarek, T. Ciach, Comparative studies of electrospinning and solution blow spinning processes for the production of nanofibrous poly(L-Lactic Acid) materials for biomedical engineering, Pol. J. Chem. Technol. 16 (2014) 43–50, https://doi.org/10.2478/pjct-2014-0028.

[13] M. Soares de Azerêdo, J.M. Marconcini, Effect of solution concentration in microfiltration properties of PLA mats produced by solution blow spinning, Polym. Eng. Sci. 61 (2021) 856–863, https://doi.org/10.1002/pen.25634.

[14] G.C. Dadol, A. Kilic, L.D. Tijing, K.J.A. Lim, L.K. Cabatingan, N.P.B. Tan, E. Stojanovska, Y. Polat, Solution blow spinning (SBS) and SBS-spun nanofibers: materials, methods, and applications, Mater. Today Commun. 25 (2020), https://doi.org/10.1016/j.mtcomm.2020.101656.

[15] B. Gupta, N. Revagade, J. Hilborn, Poly(lactic acid) fiber: an overview, Prog. Polym. Sci. (Oxf.) 32 (2007) 455–482, https://doi.org/10.1016/j.progpolymsci.2007.01.005.

[16] S. Ramanadha reddy, Dr.N. Venkatachalapathi, A review on characteristic variation in PLA material with a combination of various nano composites, Mater. Today Proc. (2023), https://doi.org/10.1016/j.matpr.2023.04.616.

[17] G. Sabbatier, D. Le Nouën, P. Chevallier, B. Durand, G. Laroche, F. Dieval, Air spun poly(lactic acid) nanofiber scaffold degradation for vascular tissue engineering: a ^{1}H NMR study, Polym. Degrad. Stab. 97 (2012) 1520–1526, https://doi.org/10.1016/j.polymdegradstab.2012.04.017.

[18] S. Arthanari, J.E. Park, J.S. Heo, D.H. Cho, M. Yang, J.S. Hwang, H. Lee, Laser surface polishing of 3D printed polylactic acid (PLA) with different levels of absorption, J. Manuf. Process 98 (2023) 265–276, https://doi.org/10.1016/j.jmapro.2023.05.034.

[19] C. Abdenour, M. Eesaee, C. Stuppa, B. Chabot, S. Barnabé, J. Bley, B. Tolnai, N. Guy, P. Nguyen-Tri, Water vapor and air barrier performance of sustainable paper coatings based on PLA and xanthan gum, Mater. Today Commun. 36 (2023), https://doi.org/10.1016/j.mtcomm.2023.106626.

[20] S. Sun, L. Gao, B. Liang, Z. Yin, S. Pan, C. Shi, C. Guo, Z. Huang, C. Chu, Y. Dong, Long-term and uniform release of magnesium ions from PLA porous composite materials oriently reinforced by Mg wires for potential bone repair application, Surf. Interfaces 40 (2023), https://doi.org/10.1016/j.surfin.2023.103018.

[21] R. Schneider, M.H.M. Facure, A.D. Alvarenga, P.A.M. Chagas, D.M. Dos Santos, D. S. Correa, Dye adsorption capacity of MoS2nanoflakes immobilized on poly(lactic acid) fibrous membranes, ACS Appl. Nano Mater. 4 (2021) 4881–4894, https://doi.org/10.1021/acsanm.1c00442.

[22] Z. Cai, C. Shen, Z. Deng, D. Wu, K. Chen, Solution blow spinning of multilayer polycaprolactone/curcumin-loaded gelatin/polycaprolactone nanofilm for slow release and bacterial inhibition, Food Hydrocoll. Health 2 (2022), https://doi.org/10.1016/j.fhfh.2022.100062.

[23] A.A. Arafa, A.A. Nada, A.Y. Ibrahim, M.K. Zahran, O.A. Hakeim, Greener therapeutic pH-sensing wound dressing based on Curcuma longa and cellulose hydrogel, Eur. Polym. J. 159 (2021), https://doi.org/10.1016/j.eurpolymj.2021.110744.

[24] M. Li, G.G.L. Yue, S.K.W. Tsui, K.P. Fung, C.B.S. Lau, Turmeric extract, with absorbable curcumin, has potent anti-metastatic effect in vitro and in vivo,

Phytomedicine 46 (2018) 131–141, https://doi.org/10.1016/j.phymed.2018.03.065.
[25] J. Jose, A.R. Pai, D.A. Gopakumar, Y. Dalvi, V. Rubi, S.G. Bhat, D. Pasquini, N. Kalarikkal, S. Thomas, Novel 3D porous aerogels engineered at nano scale from cellulose nano fibers and curcumin: an effective treatment for chronic wounds, Carbohydr. Polym. 287 (2022), https://doi.org/10.1016/j.carbpol.2022.119338.
[26] P.A.M. Chagas, R. Schneider, D.M. dos Santos, A.J.G. Otuka, C.R. Mendonça, D. S. Correa, Bilayered electrospun membranes composed of poly(lactic-acid)/natural rubber: a strategy against curcumin photodegradation for wound dressing application, React. Funct. Polym. 163 (2021), https://doi.org/10.1016/j.reactfunctpolym.2021.104889.
[27] R.L. Thangapazham, S. Sharad, R.K. Maheshwari, Skin regenerative potentials of curcumin, BioFactors 39 (2013) 141–149, https://doi.org/10.1002/biof.1078.
[28] Y. Zhao, C. Dai, Z. Wang, W. Chen, J. Liu, R. Zhuo, A. Yu, S. Huang, A novel curcumin-loaded composite dressing facilitates wound healing due to its natural antioxidant effect, Drug Des. Dev. Ther. 13 (2019) 3269–3280, https://doi.org/10.2147/DDDT.S219224.
[29] M. Ranjbar-Mohammadi, S.H. Bahrami, Electrospun curcumin loaded poly (ε-caprolactone)/gum tragacanth nanofibers for biomedical application, Int J. Biol. Macromol. 84 (2016) 448–456, https://doi.org/10.1016/j.ijbiomac.2015.12.024.
[30] A. Sharma, A. Mittal, V. Puri, P. Kumar, I. Singh, Curcumin-loaded, alginate–gelatin composite fibers for wound healing applications, 3 Biotech 10 (2020), https://doi.org/10.1007/s13205-020-02453-5.
[31] S. Peng, L. Li, J. Kong Yoong Lee, L. Tian, M. Srinivasan, S. Adams, S. Ramakrishna, Electrospun carbon nanofibers and their hybrid composites as advanced materials for energy conversion and storage, Nano Energy 22 (2016) 361–395, https://doi.org/10.1016/j.nanoen.2016.02.001.
[32] B. Zhang, Y. Liu, M. Ren, W. Li, X. Zhang, R. Vajtai, P.M. Ajayan, J.M. Tour, L. Wang, Sustainable synthesis of bright green fluorescent nitrogen-doped carbon quantum dots from alkali lignin, ChemSusChem 12 (2019) 4202–4210, https://doi.org/10.1002/cssc.201901693.
[33] É.C. Duarte, R.L. Oréfice, Self-healing interfaces of poly(methyl methacrylate) reinforced with carbon fibers decorated with carbon quantum dots, J. Appl. Polym. Sci. 138 (2021), https://doi.org/10.1002/app.49644.
[34] W. Liu, C. Ning, R. Sang, Q. Hou, Y. Ni, Lignin-derived graphene quantum dots from phosphous acid-assisted hydrothermal pretreatment and their application in photocatalysis, Ind. Crops Prod. 171 (2021), https://doi.org/10.1016/j.indcrop.2021.113963.
[35] H. Ehtesabi, Z. Hallaji, S. Najafi Nobar, Z. Bagheri, Carbon dots with pH-responsive fluorescence: a review on synthesis and cell biological applications, Microchim. Acta 187 (2020), https://doi.org/10.1007/s00604-019-4091-4.
[36] A. Cassales, L.A. Ramos, E. Frollini, Synthesis of bio-based polyurethanes from Kraft lignin and castor oil with simultaneous film formation, Int. J. Biol. Macromol. 145 (2020) 28–41, https://doi.org/10.1016/j.ijbiomac.2019.12.173.
[37] J. Wang, J. Wang, W. Xiao, Z. Geng, D. Tan, L. Wei, J. Li, L. Xue, X. Wang, J. Zhu, Lignin-derived red-emitting carbon dots for colorimetric and sensitive fluorometric detection of water in organic solvents, Anal. Methods 12 (2020) 3218–3224, https://doi.org/10.1039/d0ay00485e.
[38] M.P. Sk, A. Dutta, New-generation quantum dots as contrast agent in imaging. in: Nanomaterials in Diagnostic Tools and Devices, Elsevier, 2020, pp. 525–556, https://doi.org/10.1016/B978-0-12-817923-9.00018-3.
[39] Z. Ding, F. Li, J. Wen, X. Wang, R. Sun, Gram-scale synthesis of single-crystalline graphene quantum dots derived from lignin biomass, Green. Chem. 20 (2018) 1383–1390, https://doi.org/10.1039/c7gc03218h.
[40] P.F. Rossi, F.V. dos Santos, A.L.M.M. Alves, L.H. Semensato, L.F.R. Oliveira, D. M. dos Santos, T.P. Bianchi, N.M. Inada, S.P. Campana-Filho, R.L. Oréfice, D. S. Correa, ACS Appl. Nano Mat. 7 (2024) 23519–23531, https://doi.org/10.1021/acsanm.4c03615.
[41] W. Liu, C. Ning, R. Sang, Q. Hou, Y. Ni, Lignin-derived graphene quantum dots from phosphous acid-assisted hydrothermal pretreatment and their application in photocatalysis, Ind. Crops Prod. 171 (2021), https://doi.org/10.1016/j.indcrop.2021.113963.
[42] M.B. Stie, J.R. Gätke, F. Wan, I.S. Chronakis, J. Jacobsen, H.M. Nielsen, Swelling of mucoadhesive electrospun chitosan/polyethylene oxide nanofibers facilitates adhesion to the sublingual mucosa, Carbohydr. Polym. 242 (2020), https://doi.org/10.1016/j.carbpol.2020.116428.
[43] E. Baigorria, S. Souza dos Santos, M.R. de Moura, L.F. Fraceto, Nanocomposite hydrogels 3D printed for application in water remediation, Mater. Today Chem. 30 (2023), https://doi.org/10.1016/j.mtchem.2023.101559.
[44] R. Ravikumar, M. Ganesh, U. Ubaidulla, E. Young Choi, H. Tae Jang, Preparation, characterization, and in vitro diffusion study of nonwoven electrospun nanofiber of curcumin-loaded cellulose acetate phthalate polymer, Saudi Pharm. J. 25 (2017) 921–926, https://doi.org/10.1016/j.jsps.2017.02.004.
[45] G. Göksen, M.J. Fabra, H.I. Ekiz, A. López-Rubio, Phytochemical-loaded electrospun nanofibers as novel active edible films: characterization and antibacterial efficiency in cheese slices, Food Control 112 (2020), https://doi.org/10.1016/j.foodcont.2020.107133.
[46] D.A. Locilento, L.A. Mercante, R.S. Andre, L.H.C. Mattoso, G.L.F. Luna, P. Brassolatti, F. de, F. Anibal, D.S. Correa, Biocompatible and biodegradable electrospun nanofibrous membranes loaded with grape seed extract for wound dressing application, J. Nanomater 2019 (2019), https://doi.org/10.1155/2019/2472964.
[47] Y. Ma, X. Wang, S. Zong, Z. Zhang, Z. Xie, Y. Huang, Y. Yue, S. Liu, X. Jing, Local, combination chemotherapy in prevention of cervical cancer recurrence after surgery by using nanofibers co-loaded with cisplatin and curcumin, RSC Adv. 5 (2015) 106325–106332, https://doi.org/10.1039/c5ra17230f.
[48] R. Augustine, N. Kalarikkal, S. Thomas, An in vitro method for the determination of microbial barrier property (MBP) of porous polymeric membranes for skin substitute and wound dressing applications, Tissue Eng. Regen. Med 12 (2015) 12–19, https://doi.org/10.1007/s13770-014-0032-9.
[49] S. Wittaya-Areekul, C. Prahsarn, Development and in vitro evaluation of chitosan-polysaccharides composite wound dressings, Int J. Pharm. 313 (2006) 123–128, https://doi.org/10.1016/j.ijpharm.2006.01.027.
[50] D. Min, Y. Ahn, H.K. Lee, W. Jung, H.J. Kim, A novel optical coherence tomography-based in vitro method of anti-aging skin analysis using 3D skin wrinkle mimics, Ski. Res Technol. 29 (2023) e13354, https://doi.org/10.1111/srt.13354.
[51] J. Xiong, M.H. Grace, H. Kobayashi, M.A. Lila, Evaluation of saffron extract bioactivities relevant to skin resilience, J. Herb. Med 37 (2023), https://doi.org/10.1016/j.hermed.2023.100629.
[52] R. Corrales-Orovio, F. Carvajal, C. Holmes, M. Miranda, S. González-Itier, C. Cárdenas, C. Vera, T.L. Schenck, J.T. Egaña, Development of a photosynthetic hydrogel as potential wound dressing for the local delivery of oxygen and bioactive molecules, Acta Biomater. 155 (2023) 154–166, https://doi.org/10.1016/j.actbio.2022.11.036.
[53] C. Liu, R. Cheng, J. Guo, G. Li, H. Li, H.G. Ye, Z.Bin Liang, C.F. Wang, S. Chen, Carbon dots embedded nanofiber films: large-scale fabrication and enhanced mechanical properties, Chin. Chem. Lett. 33 (2022) 304–307, https://doi.org/10.1016/j.cclet.2021.06.073.
[54] X. Nie, S. Wu, A. Mensah, K. Lu, Q. Wei, Carbon quantum dots embedded electrospun nanofibers for efficient antibacterial photodynamic inactivation, Mater. Sci. Eng. C. 108 (2020), https://doi.org/10.1016/j.msec.2019.110377.
[55] M. Dervisevic, M. Senel, T. Sagir, S. Isik, Highly sensitive detection of cancer cells with an electrochemical cytosensor based on boronic acid functional polythiophene, Biosens. Bioelectron. 90 (2017) 6–12, https://doi.org/10.1016/j.bios.2016.10.100.
[56] M. Dervisevic, M. Senel, T. Sagir, S. Isik, Highly sensitive detection of cancer cells with an electrochemical cytosensor based on boronic acid functional polythiophene, Biosens. Bioelectron. 90 (2017) 6–12, https://doi.org/10.1016/j.bios.2016.10.100.
[57] Y. Liu, Y. Gu, X. Yan, Z. Kang, S. Lu, Y. Sun, Y. Zhang, Design of sandwich-structured ZnO/ZnS/Au photoanode for enhanced efficiency of photoelectrochemical water splitting, Nano Res. 8 (2015) 2891–2900, https://doi.org/10.1007/s12274-015-0794-y.
[58] Q. Wang, M. Wang, N. Zhang, X. Huang, X. Wang, S. Wang, A novel electrochemical sensor based on MoS2 electrospun nanofibers and polyoxometalate composite for the simultaneous detection of ractopamine and clenbuterol, Microchem. J. 189 (2023), https://doi.org/10.1016/j.microc.2023.108434.
[59] M.H.M. Facure, R.S. Andre, R.M. Cardoso, L.A. Mercante, D.S. Correa, Electrochemical and optical dual-mode detection of phenolic compounds using MnO2/GQD nanozyme, Electro Acta 441 (2023), https://doi.org/10.1016/j.electacta.2022.141777.
[60] P.A.M. Chagas, R. Schneider, D.M. dos Santos, A.J.G. Otuka, C.R. Mendonça, D. S. Correa, Bilayered electrospun membranes composed of poly(lactic-acid)/natural rubber: a strategy against curcumin photodegradation for wound dressing application, React. Funct. Polym. 163 (2021), https://doi.org/10.1016/j.reactfunctpolym.2021.104889.
[61] P. Pankongadisak, S. Sangklin, P. Chuysinuan, O. Suwantong, P. Supaphol, The use of electrospun curcumin-loaded poly(L-lactic acid) fiber mats as wound dressing materials, J. Drug Deliv. Sci. Technol. 53 (2019), https://doi.org/10.1016/j.jddst.2019.06.018.
[62] T. Krasian, W. Punyodom, R. Molloy, P.D. Topham, B.J. Tighe, A. Mahomed, T. Chaiwarit, P. Panraksa, P. Rachtanapun, K. Jantanasakulwong, P. Worajittiphon, Low cytotoxicity, antibacterial property, and curcumin delivery performance of toughness-enhanced electrospun composite membranes based on poly(lactic acid) and MAX phase (Ti3AlC2), Int J. Biol. Macromol. 262 (2024), https://doi.org/10.1016/j.ijbiomac.2024.129967.
[63] L.I. Ramdhanie, S.R. Aubuchon, E.D. Boland, D.C. Knapp, C.P. Barnes, D. G. Simpson, G.E. Wnek, G.L. Bowlin, Thermal and mechanical characterization of electrospun blends of poly(lactic acid) and poly(glycolic acid), Polym. J. 38 (2006) 1137–1145, https://doi.org/10.1295/polymj.PJ2006062.
[64] S.M. Oliveira, N.M. Alves, J.F. Mano, Cell interactions with superhydrophilic and superhydrophobic surfaces, J. Adhes. Sci. Technol. 28 (2014) 843–863, https://doi.org/10.1080/01694243.2012.697776.
[65] C. Gandhimathi, J.R. Venugopal, V. Bhaarathy, S. Ramakrishna, S.D. Kumar, , Biocomposite nanofibrous strategies for the controlled release of biomolecules for skin tissue regeneration, Int J. Nanomed. 9 (2014) 4709–4722, https://doi.org/10.2147/IJN.S65335.
[66] L. Moradkhannejhad, M. Abdouss, N. Nikfarjam, M.H. Shahriari, V. Heidary, The effect of molecular weight and content of PEG on in vitro drug release of electrospun curcumin loaded PLA/PEG nanofibers, J. Drug Deliv. Sci. Technol. 56 (2020), https://doi.org/10.1016/j.jddst.2020.101554.
[67] Y. Zhao, Q. Lu, J. Wu, Y. Zhang, J. Guo, J. Yu, X. Shu, Q. Chen, Flexible, robust and self-peeling PLA/AgNWs nanofiber membranes with photothermally antibacterial properties for wound dressing, Appl. Surf. Sci. 615 (2023), https://doi.org/10.1016/j.apsusc.2022.156284.
[68] M. Ranjbar-Mohammadi, S.H. Bahrami, Electrospun curcumin loaded poly (ε-caprolactone)/gum tragacanth nanofibers for biomedical application, Int J. Biol. Macromol. 84 (2016) 448–456, https://doi.org/10.1016/j.ijbiomac.2015.12.024.
[69] C. Gandhimathi, J.R. Venugopal, V. Bhaarathy, S. Ramakrishna, S.D. Kumar, Biocomposite nanofibrous strategies for the controlled release of biomolecules for

skin tissue regeneration, Int J. Nanomed. 9 (2014) 4709–4722, https://doi.org/10.2147/IJN.S65335.
[70] O. Yu, K.H. Kim, Lignin to materials: a focused review on recent novel lignin applications, Appl. Sci. 10 (2020), https://doi.org/10.3390/app10134626.
[71] Y. Zheng, F. Yao, F. Chen, Curcumin-loaded electrospun peanut protein isolate/poly-L-lactic acid nanofibre membranes: preparation and characterisation and release behaviour, LWT 169 (2022), https://doi.org/10.1016/j.lwt.2022.113978.
[72] D.A. Locilento, L.A. Mercante, R.S. Andre, L.H.C. Mattoso, G.L.F. Luna, P. Brassolatti, F. de, F. Anibal, D.S. Correa, Biocompatible and biodegradable electrospun nanofibrous membranes loaded with grape seed extract for wound dressing application, J. Nanomater 2019 (2019) 1–11, https://doi.org/10.1155/2019/2472964.
[73] D. Sharma, B.K. Satapathy, Understanding release kinetics and collapse proof suture retention response of curcumin loaded electrospun mats based on aliphatic polyesters and their blends, J. Mech. Behav. Biomed. Mater. 120 (2021) 104556, https://doi.org/10.1016/j.jmbbm.2021.104556.
[74] C. Sachdeva, K. Satyamoorthy, T.S. Murali, Microbial interplay in skin and chronic wounds, Curr. Clin. Microbiol Rep. 9 (2022) 21–31, https://doi.org/10.1007/s40588-022-00180-4.
[75] Y. Zhang, J. Yu, H. Zhang, Y. Li, L. Wang, Nanofibrous dressing: potential alternative for fighting against antibiotic-resistance wound infections, J. Appl. Polym. Sci. 139 (2022), https://doi.org/10.1002/app.52178.
[76] S. Homaeigohar, A.R. Boccaccini, Antibacterial biohybrid nanofibers for wound dressings, Acta Biomater. 107 (2020) 25–49, https://doi.org/10.1016/j.actbio.2020.02.022.
[77] S. Ramanadha reddy, Dr.N. Venkatachalapathi, A review on characteristic variation in PLA material with a combination of various nano composites, Mater. Today Proc. (2023), https://doi.org/10.1016/j.matpr.2023.04.616.
[78] G. Perumal, S. Pappuru, D. Chakraborty, A. Maya Nandkumar, D.K. Chand, M. Doble, Synthesis and characterization of curcumin loaded PLA—hyperbranched polyglycerol electrospun blend for wound dressing applications, Mater. Sci. Eng. C. 76 (2017) 1196–1204, https://doi.org/10.1016/j.msec.2017.03.200.
[79] D. Rai, J.K. Singh, N. Roy, D. Panda, Curcumin inhibits FtsZ assembly: an attractive mechanism for its antibacterial activity, Biochem. J. 410 (2008) 147–155, https://doi.org/10.1042/BJ20070891.
[80] S.Y. Teow, K. Liew, S.A. Ali, A.S.B. Khoo, S.C. Peh, Antibacterial action of curcumin against Staphylococcus aureus: a brief review, J. Trop. Med 2016 (2016), https://doi.org/10.1155/2016/2853045.
[81] A.G. Morena, A. Bassegoda, M. Natan, G. Jacobi, E. Banin, T. Tzanov, Antibacterial properties and mechanisms of action of sonoenzymatically synthesized lignin-based nanoparticles, ACS Appl. Mater. Interfaces 14 (2022) 37270–37279, https://doi.org/10.1021/acsami.2c05443.
[82] A.G. Morena, T. Tzanov, Antibacterial lignin-based nanoparticles and their use in composite materials, Nanoscale Adv. 4 (2022) 4447–4469, https://doi.org/10.1039/d2na00423b.
[83] K. Li, W. Zhong, P. Li, J. Ren, K. Jiang, W. Wu, Antibacterial mechanism of lignin and lignin-based antimicrobial materials in different fields, Int J. Biol. Macromol. 252 (2023), https://doi.org/10.1016/j.ijbiomac.2023.126281.
[84] C.A. Marangon, C.G. Otoni, P.C. Bertuso, P.F. Rossi, D.M. dos Santos, T. V. Lourençon, V.C.A. Martins, A.M.G. Plepis, L.H.C. Mattoso, M. Nitschke, Side-stream lignins: potential antioxidant and antimicrobial agents in milk, Food Res. Int. 180 (2024), https://doi.org/10.1016/j.foodres.2024.114091.